Electronic Supplementary Information (ESI)

New bis-pyrazole-bis-acetate based coordination complexes: influence of counter-anions and metal ions on the supramolecular structures

Afaf Oulmidi [1,2], Smaail Radi [1]*, Haralampos N. Miras [3] , Nayarassery N. Adarsh [4] and Yann Garcia [2]*

1 LCAE, Department of Chemistry, Faculty of Sciences, University Mohamed I, BP 524, 60 000 Oujda, Morocco; afafoulmidi.ao@gmail.com
2 Institute of Condensed Matter and Nanosciences, Molecular Chemistry, Materials and Catalysis (IMCN/MOST), Université catholique de Louvain, Place Louis Pasteur 1, 1348 Louvain-la-Neuve, Belgium.
3 School of Chemistry, Joseph Black Building, Complex Chemical Systems group, University of Glasgow, Glasgow, UK; Charalampos.Moiras@glasgow.ac.uk
4 School of Chemical Sciences, Mahatma Gandhi University, Kottayam, 686560, Kerala, India; adarshnn@gmail.com
* Correspondence: s.radi@ump.ac.ma; yann.garcia@uclouvain.be; Fax: +32-10472330

Table of Contents

1. NMR of ligands (^{1}H and ^{13}C) and of **1** (^{1}H)……..S2-S5
2. Scheme S1 - Various possible conformations of **L**……..S6
3. ESI–Mass spectrometry of ligands and complexes…….....S9
4. FT-IR spectra of Ligands and Coordination compounds……S11–S13
5. UV-visible spectra of Ligands and Coordination compounds……S14
6. Hydrogen bonding parameters (Table S2)……S15
7. Shape index and curvedness of **B**, **L**, **1**, **2** and **3**……....S16-S19
8. 2D Fingerprint plots of **B**, **L**, **1**, **2** and **3**……S20–S24
9. TGA of **L**, **1**, **2** and **3**……..S25–S27
10. Ortep plots of **B**, **L**, **1**, **2** and **3**……..S28

1. NMR of Ligands

A (^{1}H and ^{13}C)

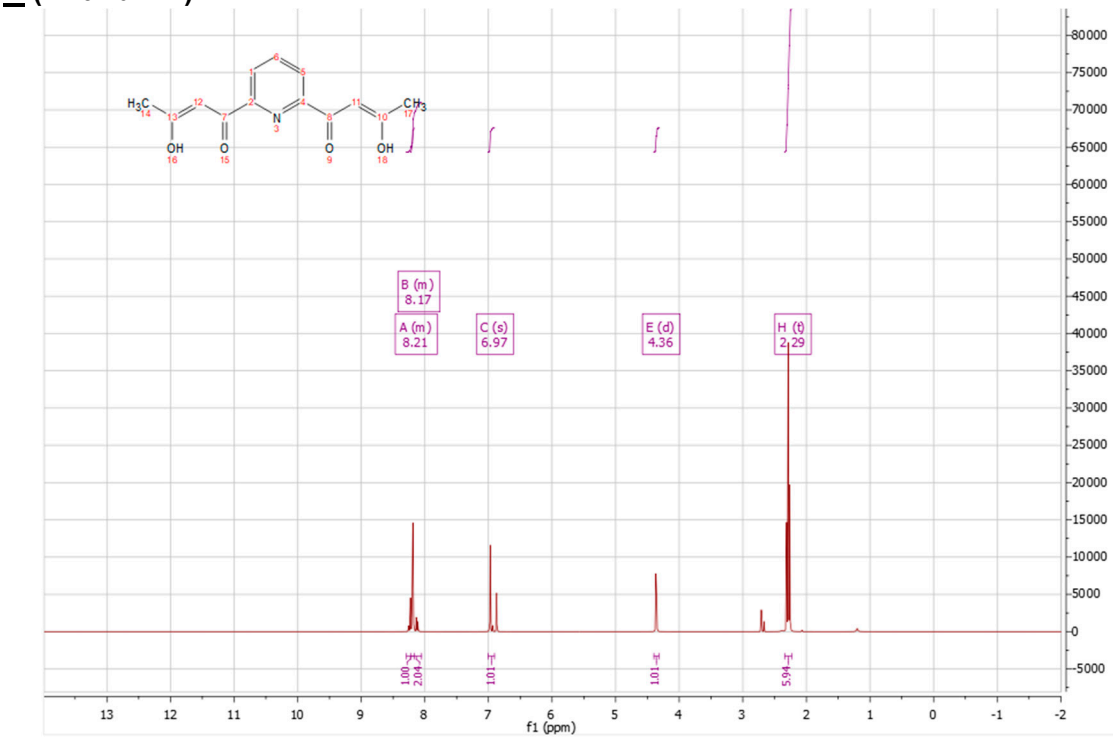

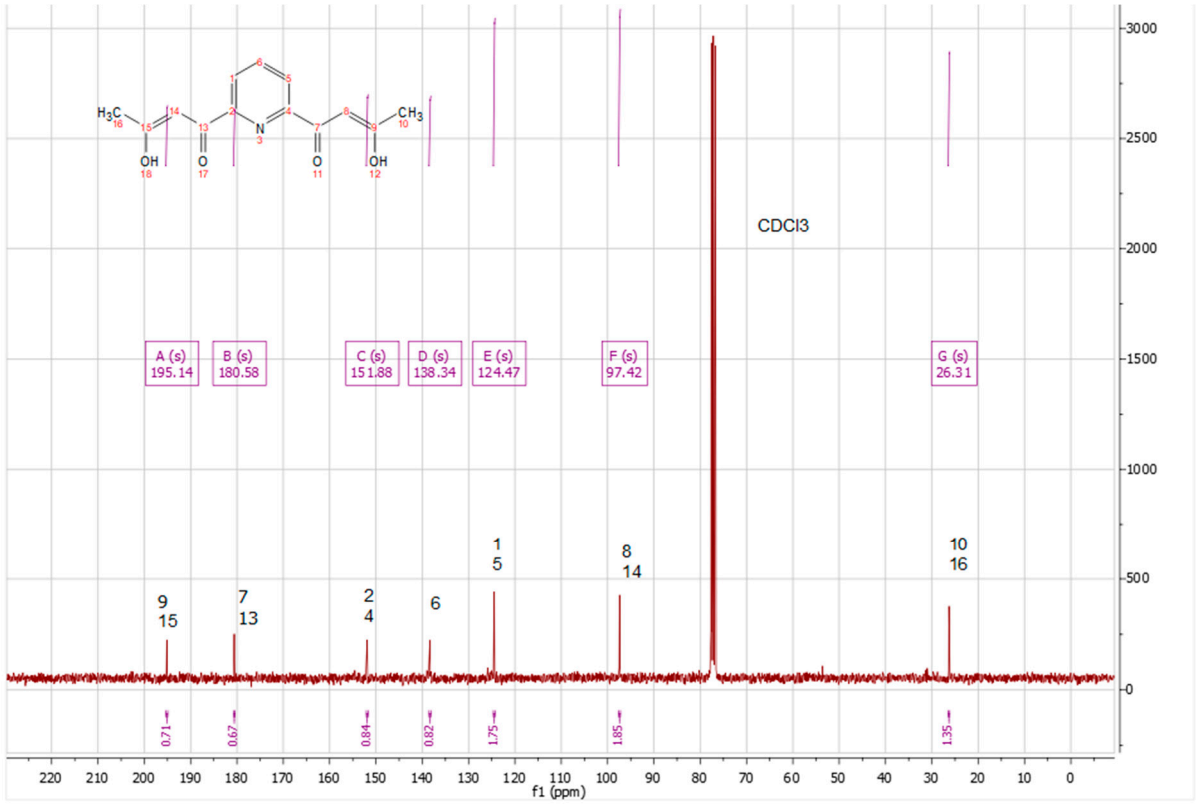

B (^{1}H and ^{13}C)

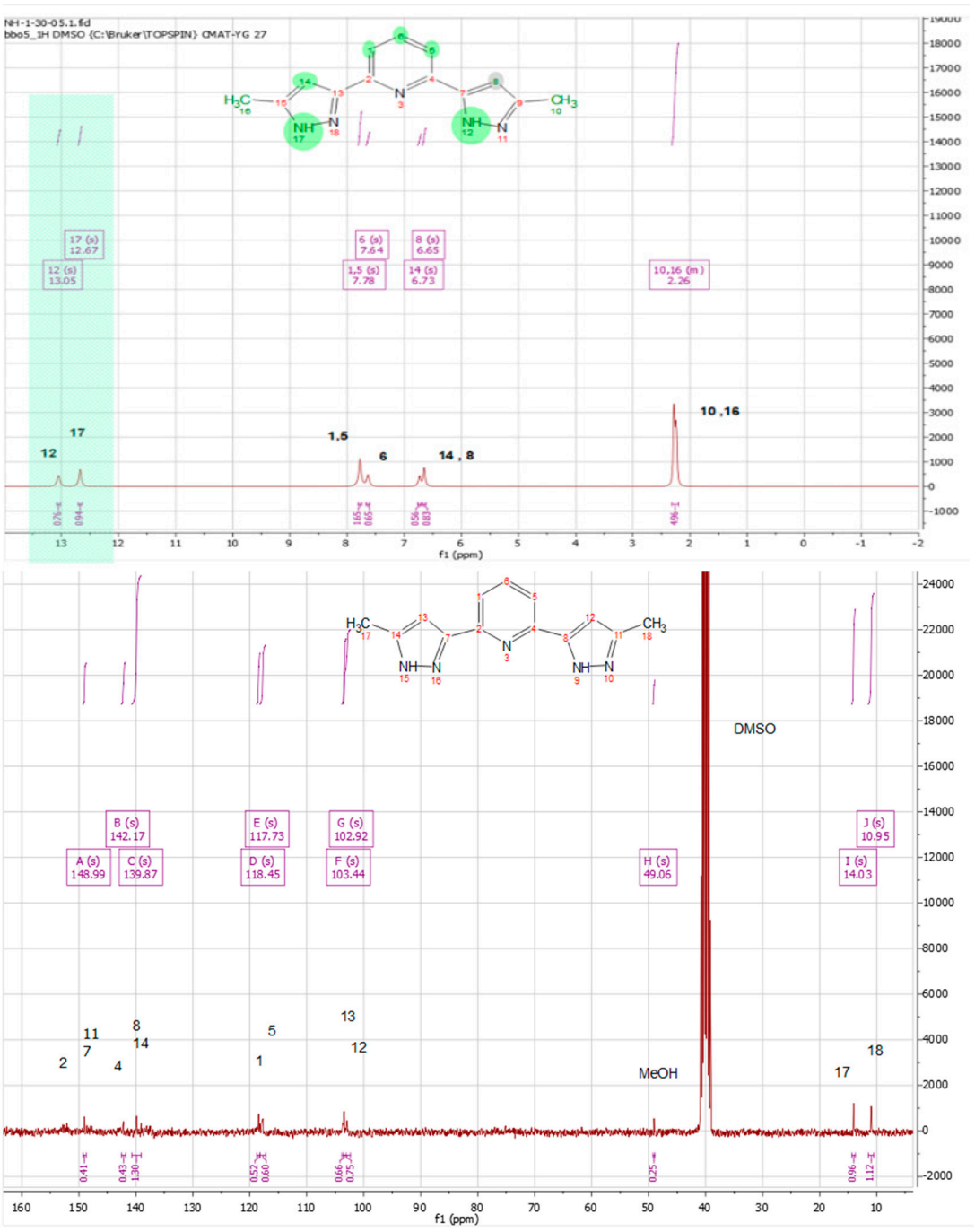
NH-1-30-05.1.fd
bbo5_1H DMSO {C:\Bruker\TOPSPIN} CMAT-YG 27
17 (s) 12.67
12 (s) 13.05
6 (s) 7.64
8 (s) 6.65
1,5 (s) 7.78
14 (s) 6.73
10,16 (m) 2.26
17
12
1,5
6
14 , 8
10 ,16
f1 (ppm)
B (s) 142.17
A (s) 148.99
C (s) 139.87
E (s) 117.73
D (s) 118.45
G (s) 102.92
F (s) 103.44
H (s) 49.06
J (s) 10.95
I (s) 14.03
DMSO
MeOH
f1 (ppm)

L (^{1}H and ^{13}C)

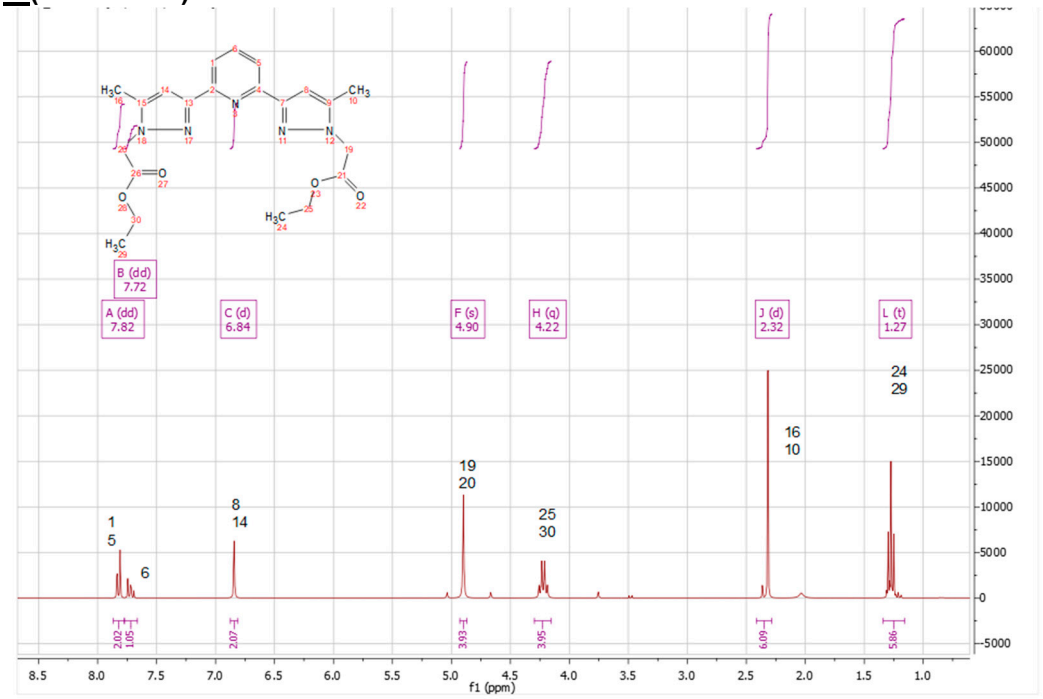
B (dd)
7.72
A (dd)
7.82
C (d)
6.84
F (s)
4.90
H (q)
4.22
J (d)
2.32
L (t)
1.27
f1 (ppm)

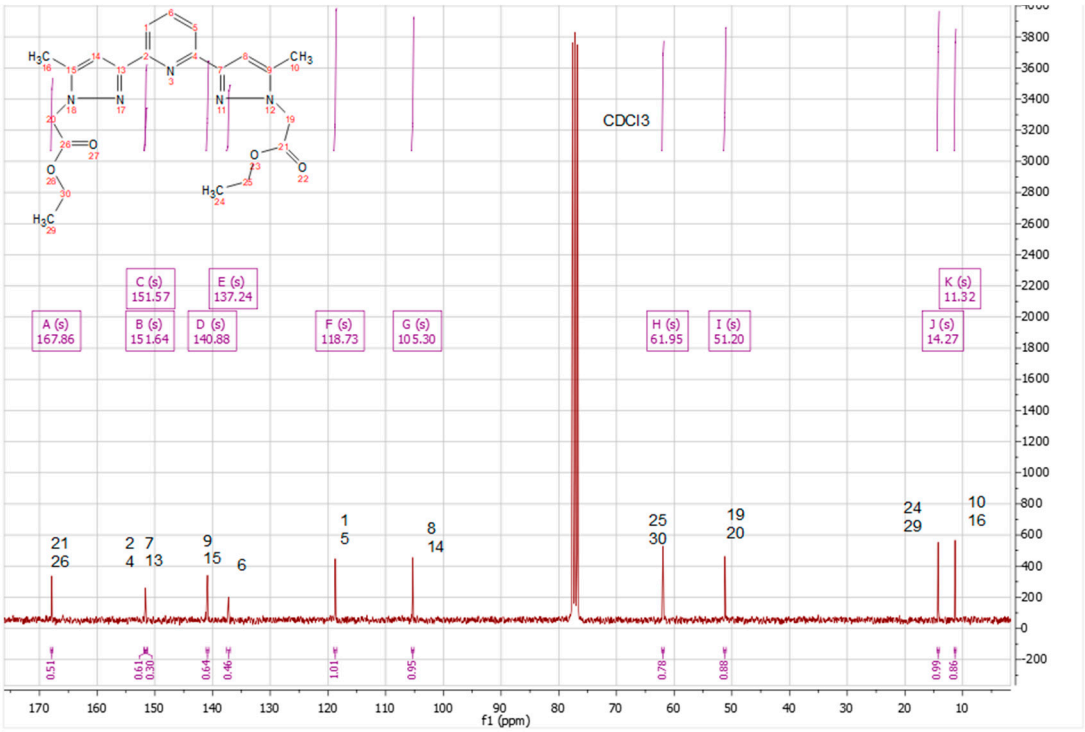
CDCl3
C (s)
151.57
E (s)
137.24
A (s)
167.86
B (s)
151.64
D (s)
140.88
F (s)
118.73
G (s)
105.30
H (s)
61.95
I (s)
51.20
K (s)
11.32
J (s)
14.27
f1 (ppm)

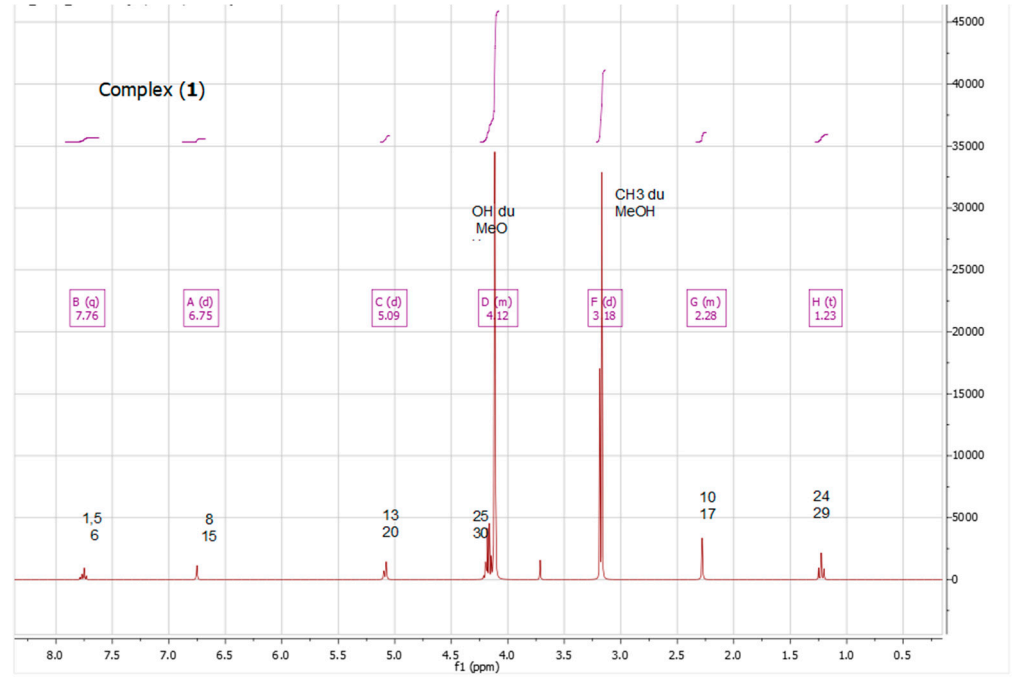
Complex (1)
OH du MeO
CH3 du MeOH
B (q) 7.76
A (d) 6.75
C (d) 5.09
D (m) 4.12
F (d) 3.18
G (m) 2.28
H (t) 1.23
1,5 6
8 15
13 20
25 30
10 17
24 29
f1 (ppm)

2. Scheme S1 - Various possible conformations of L.

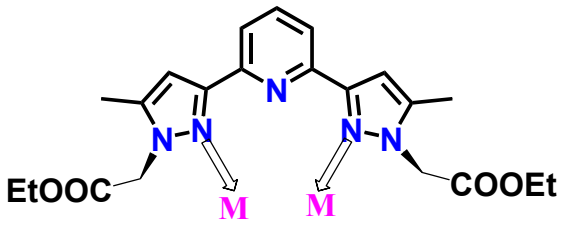

syn-syn-syn-syn-syn
(A)

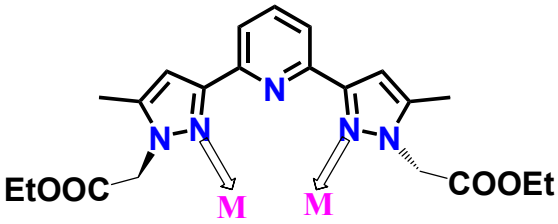

syn-syn-syn-syn-anti
(B)

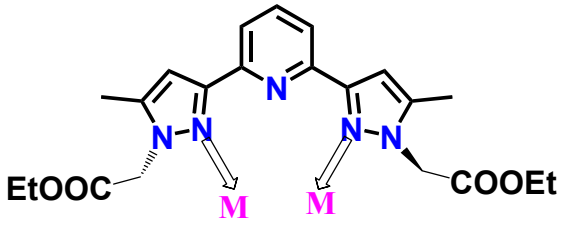

anti-syn-syn-syn-syn
(C)

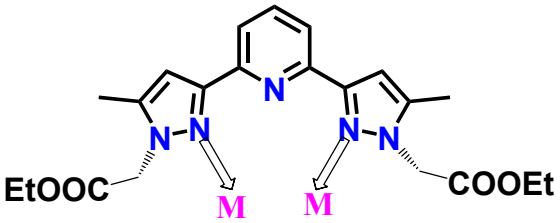

anti-syn-syn-syn-anti
(D)

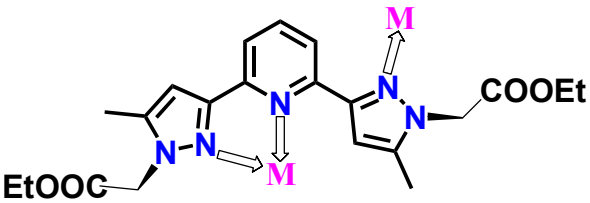

syn-syn-syn-anti-syn
(E)

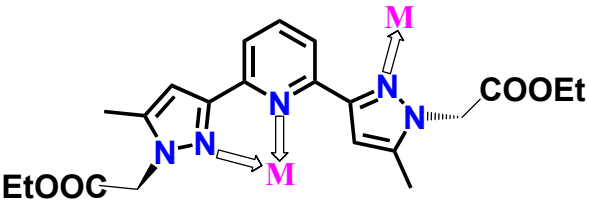

syn-syn-syn-anti-anti
(F)

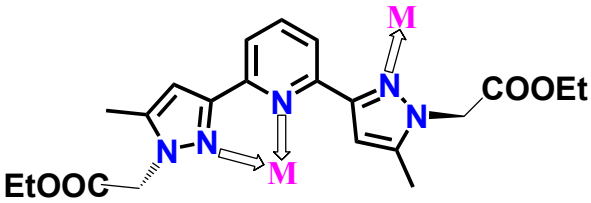

anti-syn-syn-anti-syn
(G)

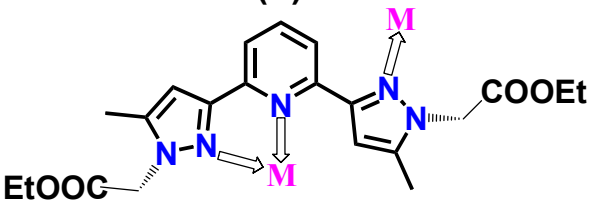

anti-syn-syn-anti-anti
(H)

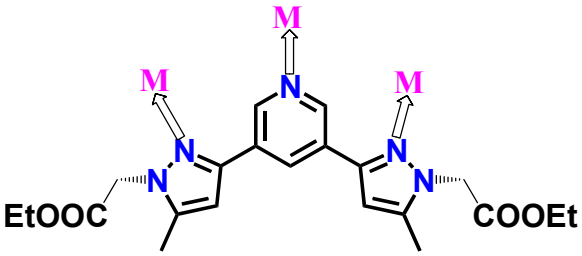

anti-anti-anti-anti-anti

(I)

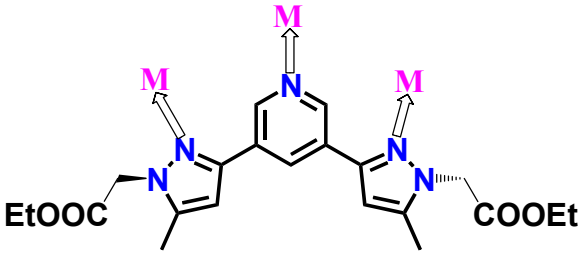

syn-anti-anti-anti-anti

(J)

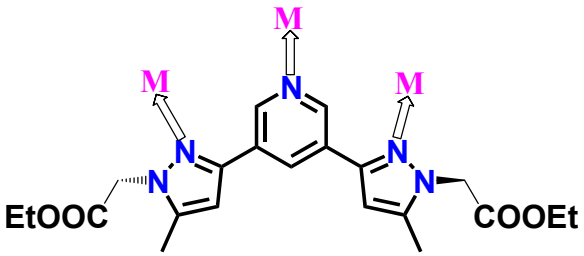

syn-anti-anti-anti-anti

(K)

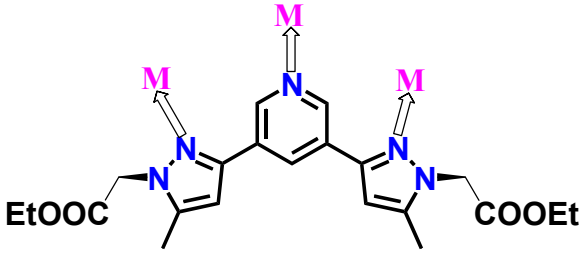

syn-anti-anti-anti-syn

(L)

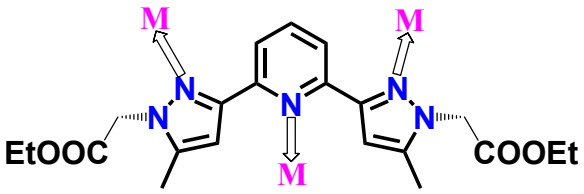

anti-anti-syn-anti-anti

(M)

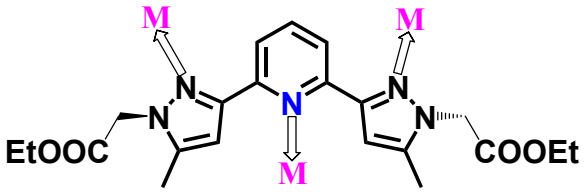

syn-anti-syn-anti-anti

(N)

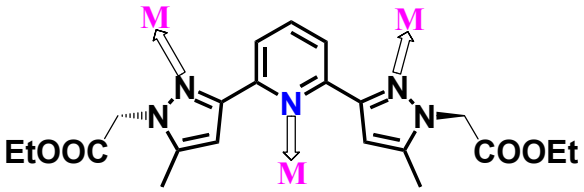

anti-anti-syn-anti-syn

(O)

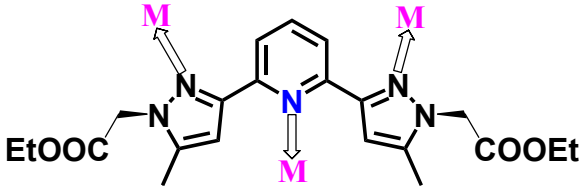

syn-anti-syn-anti-syn

(P)

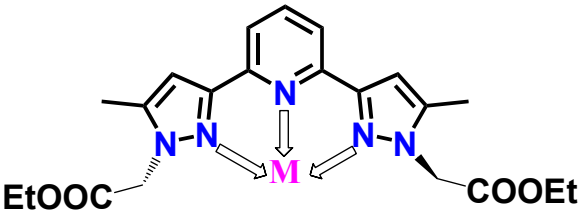

anti-syn-syn-syn-syn
(Q)

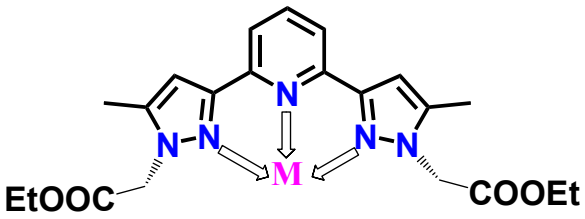

anti-syn-syn-syn-anti
(R)

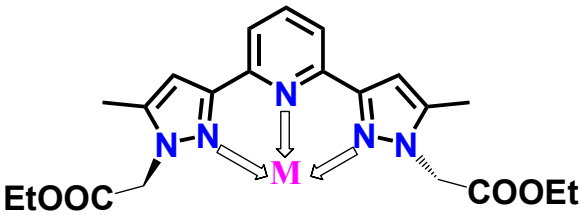

syn-syn-syn-syn-anti
(S)

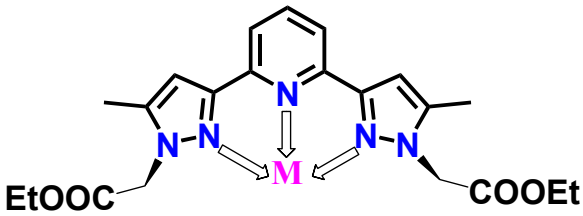

syn-syn-syn-syn-syn
(T)

3. ESI–Mass spectrometry of ligands and complexes

A

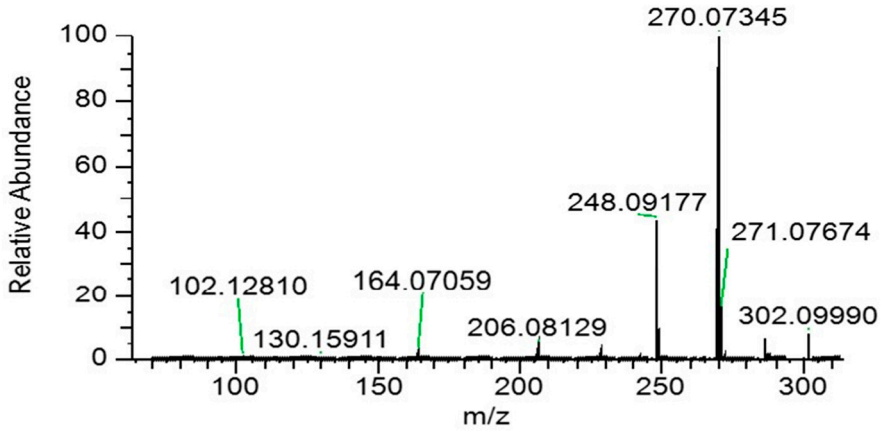

B

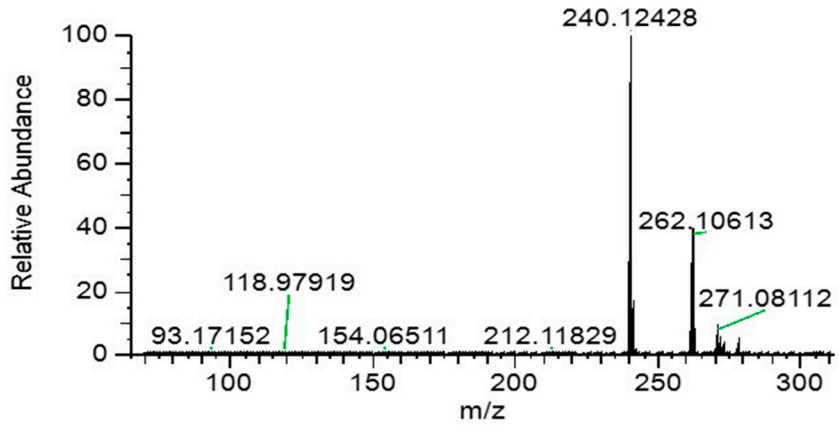

L

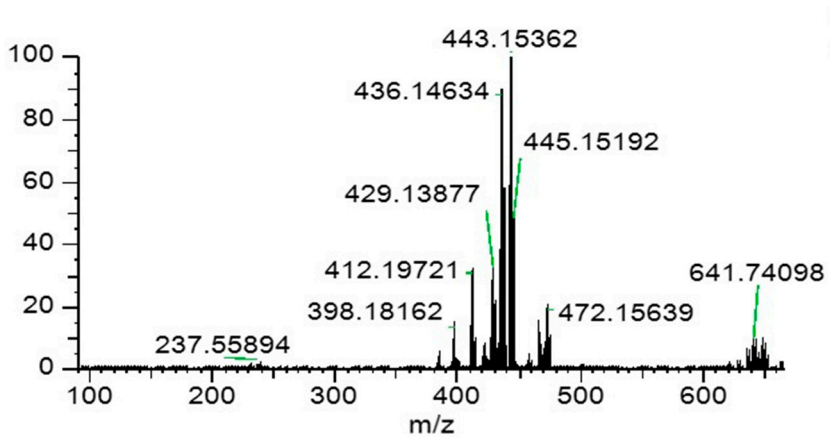

$[Zn(L)_2](BF_4)_2$ (1)

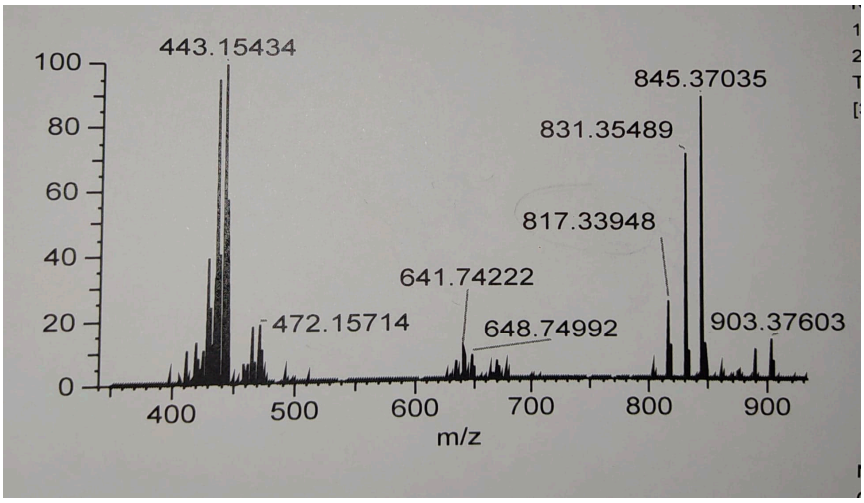

$[MnLCl_2]$ (2)

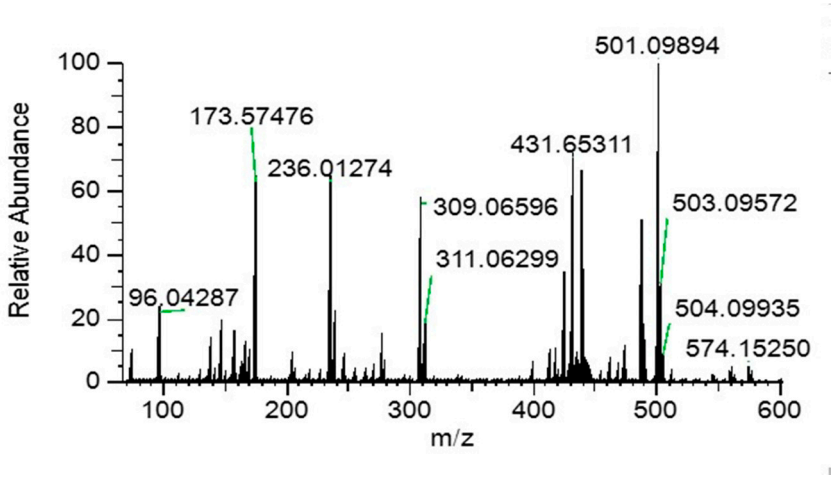

[$CdLCl_2$] (3)

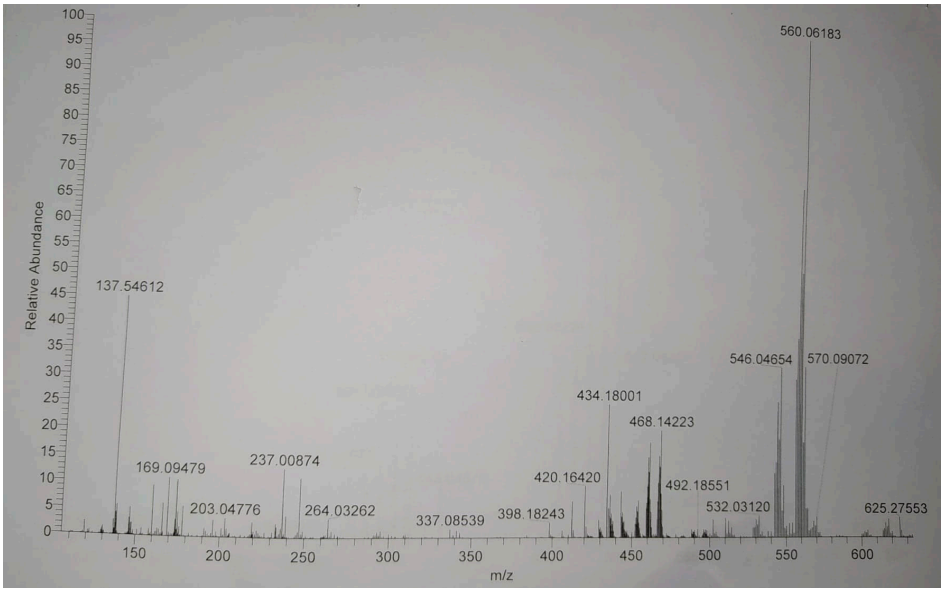

4. FT-IR spectroscopy comparison plot of L with coordination compounds

FT-IR spectra of **B** and **L** contain characteristic bands at 3133 and 1736 cm^{-1}, corresponding to N–H and C=O of the pyrazole and acetate groups, respectively. The O–H stretching frequency at 3217 cm^{-1} was also shown by the FT-IR spectra of **B**, which is attributed to a lattice included ethanol molecule. The FT-IR spectra of **B** and **L** also revealed aromatic C–H stretching frequencies at 2978 cm^{-1} and 2993 cm^{-1}, respectively. FT-IR spectra of **1**, **2** and **3** contain a medium band at 2992, 2981 and 2985 cm^{-1}, respectively, which is attributed to the aromatic C–H stretching of the metal bound ligand **L**. Another important and strong characteristic peak of C=O stretching of ethyl acetate group of metal bound **L** was found at 1736, 1747 and 1760 cm^{-1}, in the corresponding FT-IR spectra of **1**, **2** and **3**, respectively. Aromatic C–H (**1** – 829 cm^{-1}, **2** – 819 cm^{-1} and **3** – 806 cm^{-1}) and C=C (**1** – 1502 cm^{-1}, **2** – 1504 cm^{-1} and **3** – 1508 cm^{-1}) bending vibration frequency peaks were also found in all the three coordination compounds. Moreover, the medium intense FT-IR band at 1026 cm^{-1} (υ B–F) indicated the presence of tetrafluoroborate anion in the crystalline sample of **1**.

L and 1

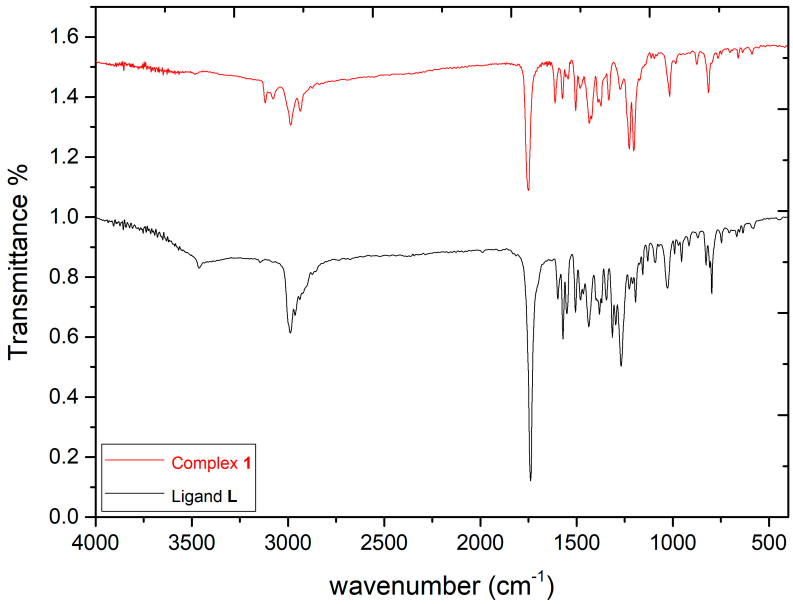
Transmittance %
wavenumber (cm-1)
Complex 1
Ligand L

L and 2

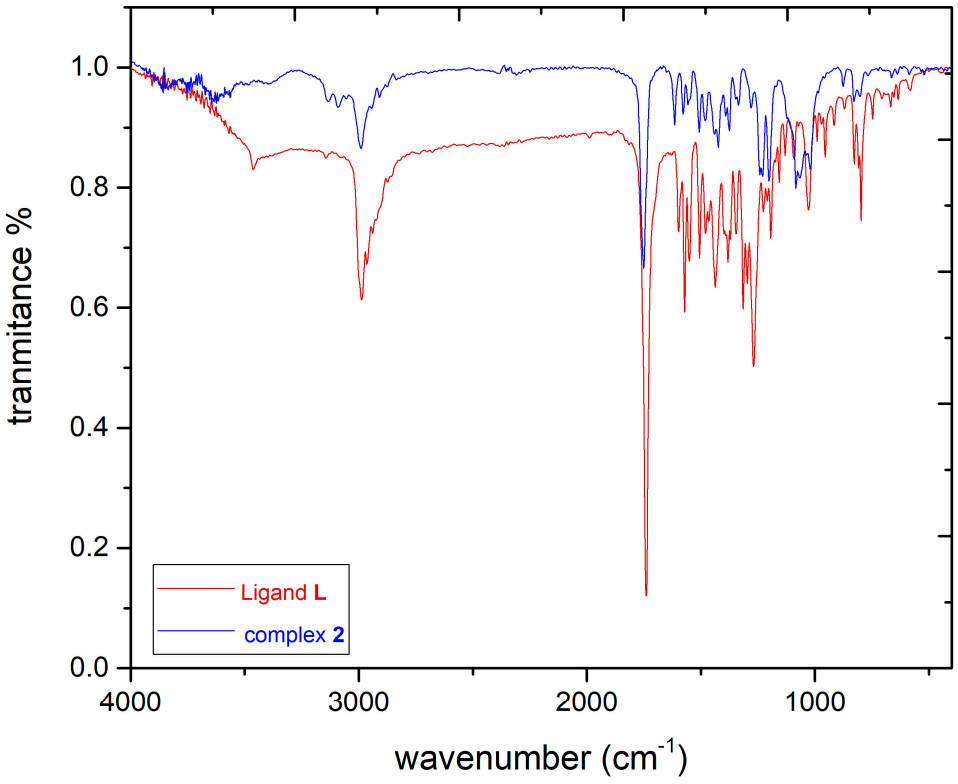
tranmitance %
wavenumber (cm-1)
Ligand L
complex 2

L and 3

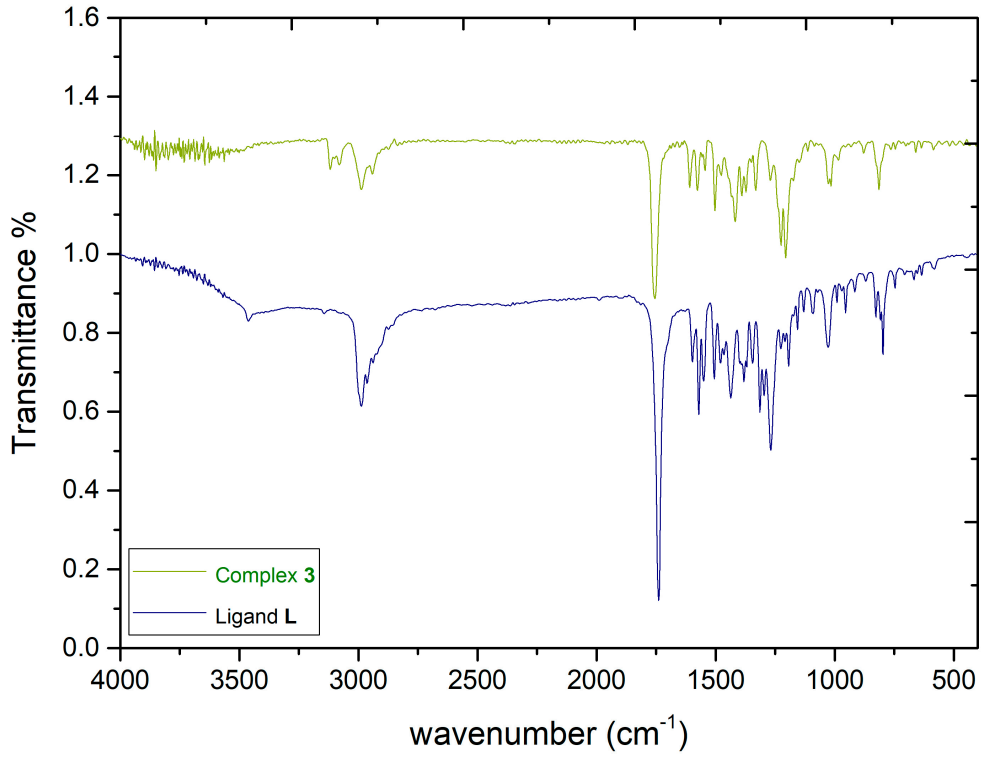
Transmittance %
wavenumber (cm-1)
Complex 3
Ligand L
1.6
1.4
1.2
1.0
0.8
0.6
0.4
0.2
0.0
4000
3500
3000
2500
2000
1500
1000
500

5. UV-visible spectroscopy comparison plot of L with 1-3

The electronic spectra of coordination compounds showed absorption bands exclusively in the UV region, corresponding to intra-ligand transitions such as π-π* and n-π*. Similar bands were also observed in the spectra of all coordination compounds, although they are red-shifted.

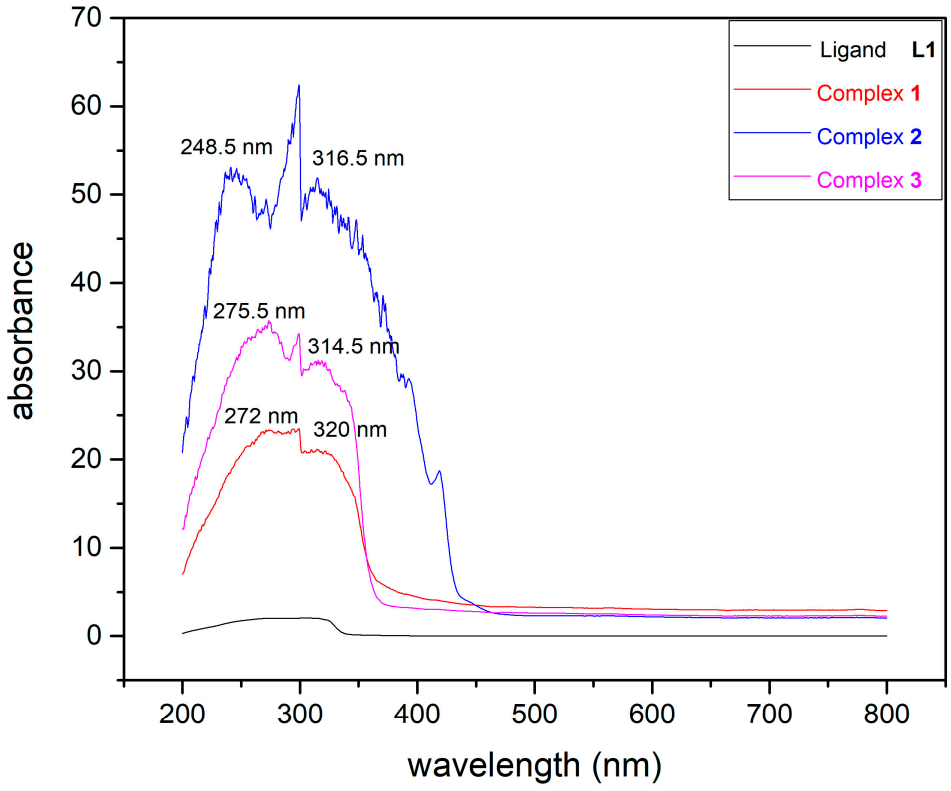

6. Table S1: Hydrogen bonding parameters of ligands **B**, **L** and **1**, **2** and **3**.

D–H···A	D–H (Å)	H···A (Å)	D···A (Å)	D–H···A (°)	Symmetry operation for A
B					
N(8)–H(8)···O(23)	0.86	1.90	2.761(8)	173	x, y, z
N(8)–H(8)···O(23B)	0.86	2.03	2.866(16)	162	x, y, z
N(15)–H(15)···N(9)	0.86	2.04	2.887(4)	167	1/2+x, 3/2-y, 1-z
O(23)–H(23)···N(14)	0.82	2.09	2.909(8)	177	x, y, z
L					
C(13)–H(13A)···N(11)	0.97	2.61	3.562(6)	166	-x, 2-y, 2-z
C(13)–H(13B)···O(27)	0.97	2.42	3.142(5)	131	x, y, 1+z
C(25)–H(25A)···O(15)	0.97	2.48	3.281(10)	140	1+x, y, -1+z
C(25)–H(25A)···O(15B)	0.97	2.29	3.17(5)	151	1+x, y, -1+z
1					
C(13)–H(13)···O(3)	0.95	2.51	3.176(4)	127	x, 3/2-y, 1/2+z
C(55)–H(55)···O(16)	0.95	2.57	3.243(5)	128	x, 1/2-y, 1/2+z
C(11)–H(11)···F(8)	0.95	2.28	3.202(4)	163	x, 3/2-y, 1/2+z
C(12)–H(12)···F(5)	0.95	2.51	3.149(5)	125	x, 3/2-y, 1/2+z
C(19)–H(19B)···F(1)	0.99	2.21	3.195(4)	174	2-x, 1/2+y, 1/2-z
C(43)–H(43B)···F(5)	0.99	2.38	3.198(5)	140	x, y, z
C(46)–H(46B)···F(7)	0.99	2.39	3.137(10)	132	x, 3/2-y, -1/2+z
C(55)–H(55)···F(10)	0.95	2.53	3.156(4)	124	x, y, z
C(78)–H(78)···F(16)	0.95	2.47	3.085(4)	123	x, y, -1+z
C(83)–H(83A)···F(3)	0.98	2.54	3.183(5)	123	x, y, z
C(85)–H(85B)···F(3)	0.99	2.30	3.206(4)	151	x, y, z
2					
C(18)–H(18A)···Cl(1)	0.99	2.57	3.466(5)	151	x, -3/2-y, -1/2+z
C(46)–H(46A)···Cl(5)	0.99	2.63	3.541(5)	153	-x, -1-y, 1-z
C(43)–H(43B)···O(3)	0.98	2.58	3.227(10)	123	-1+x, y, z
C(52)–H(52)···O(10)	0.95	2.56	3.204(9)	125	-x, 1/2+y, 1/2-z
3					
C(7)–H(7A)···O(1)	0.98	2.39	3.258(6)	147	1/2-x, y, 3/2-z

7. Shape index and curvedness

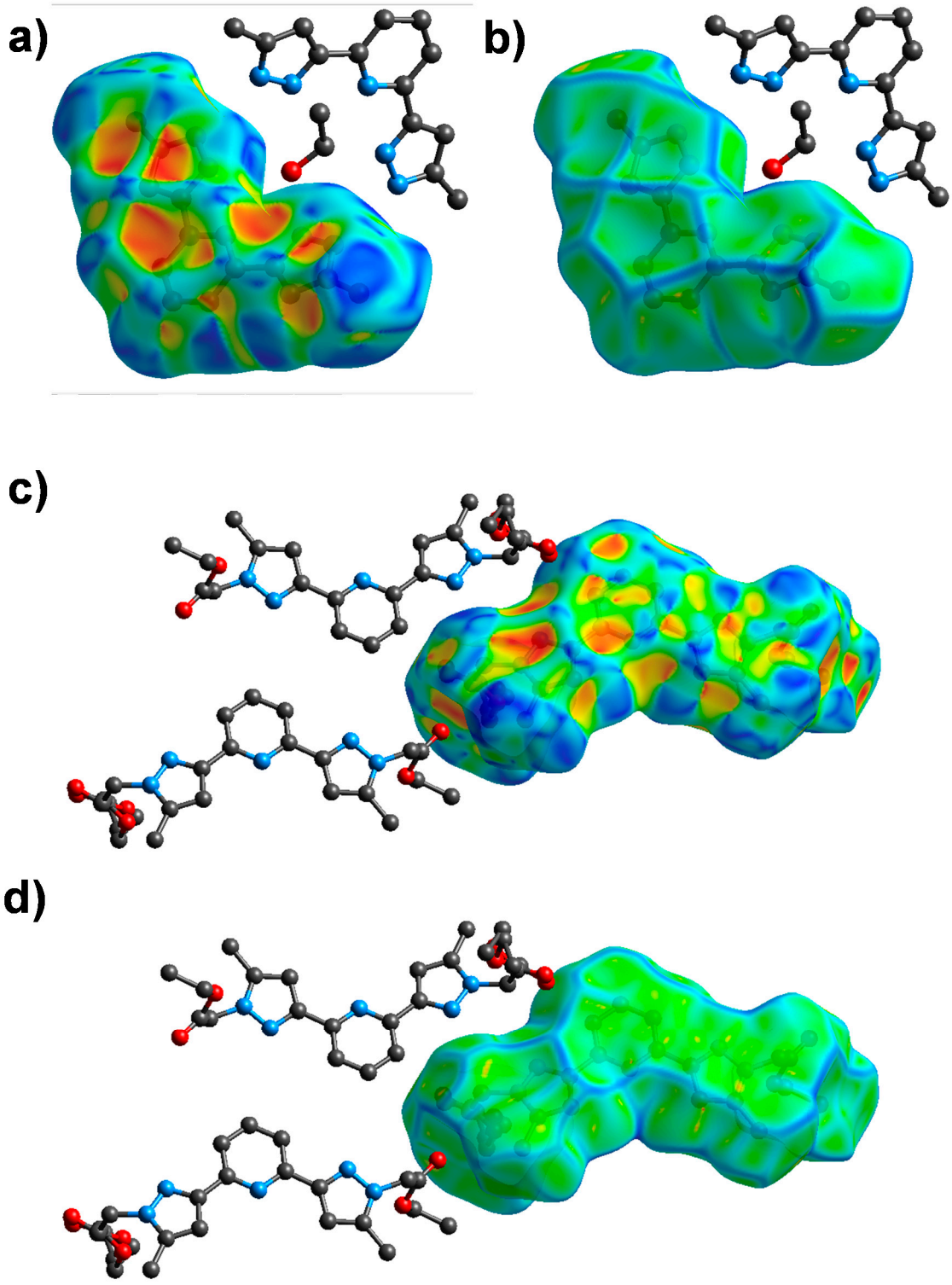

Figure S1: shape index of **B** (a) and **L** (c); curvedness of **B** (b) and **L** (d).

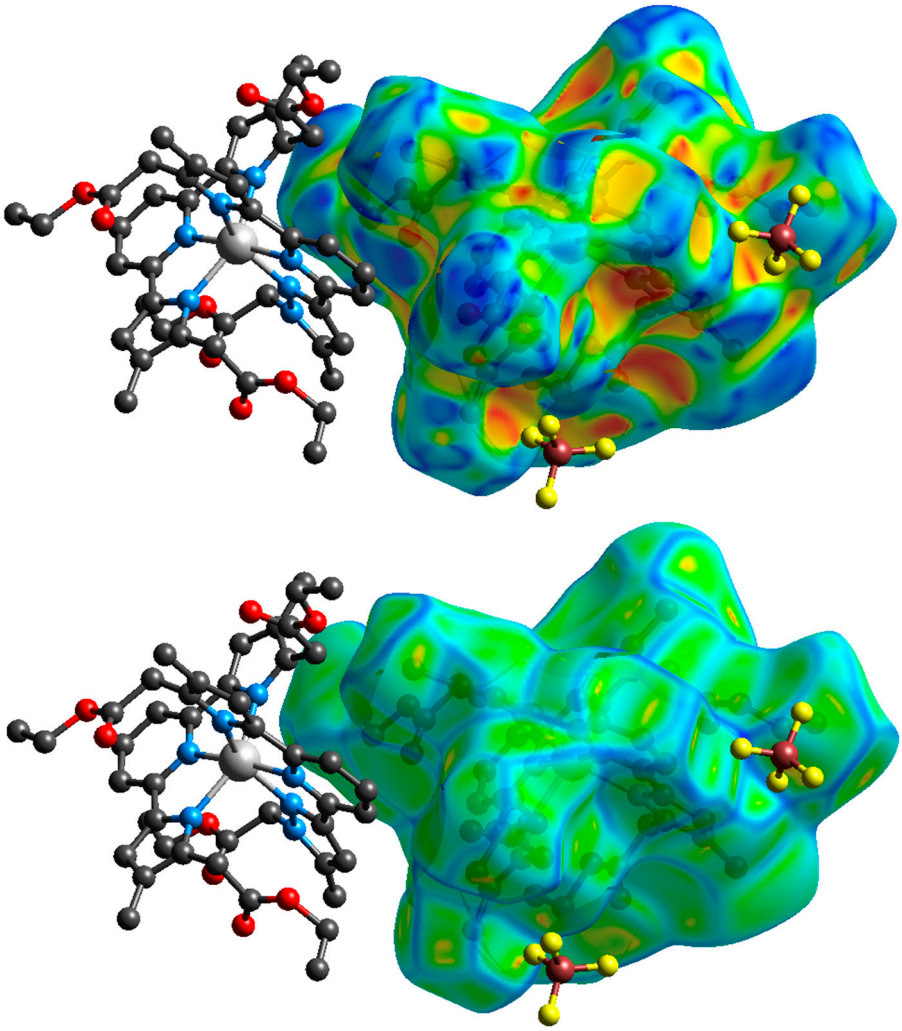

Figure S2: shape index (*top*) and curvedness (*bottom*) of **1.**

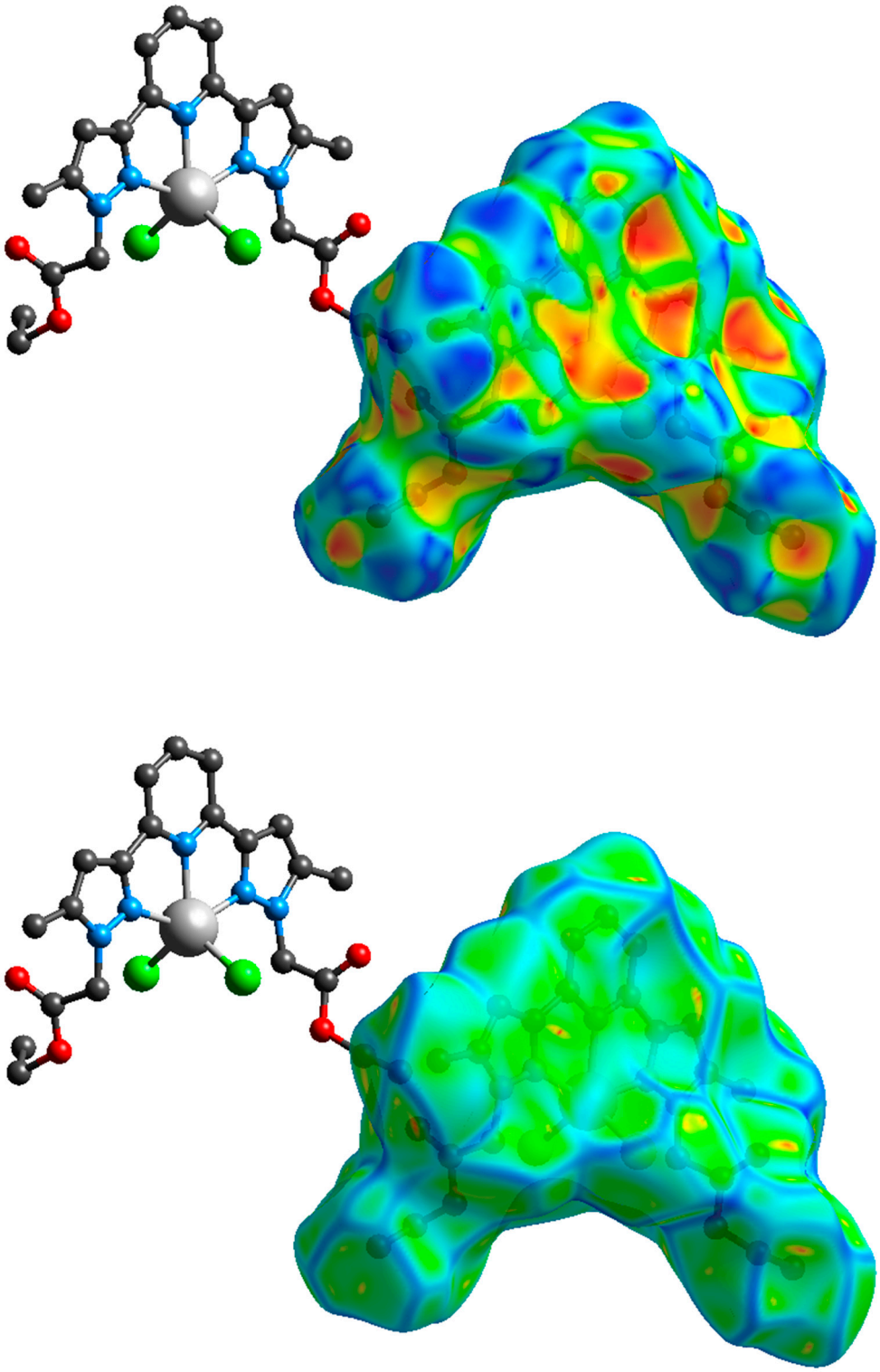

Figure S3: shape index (*top*) and curvedness (*bottom*) of **2.**

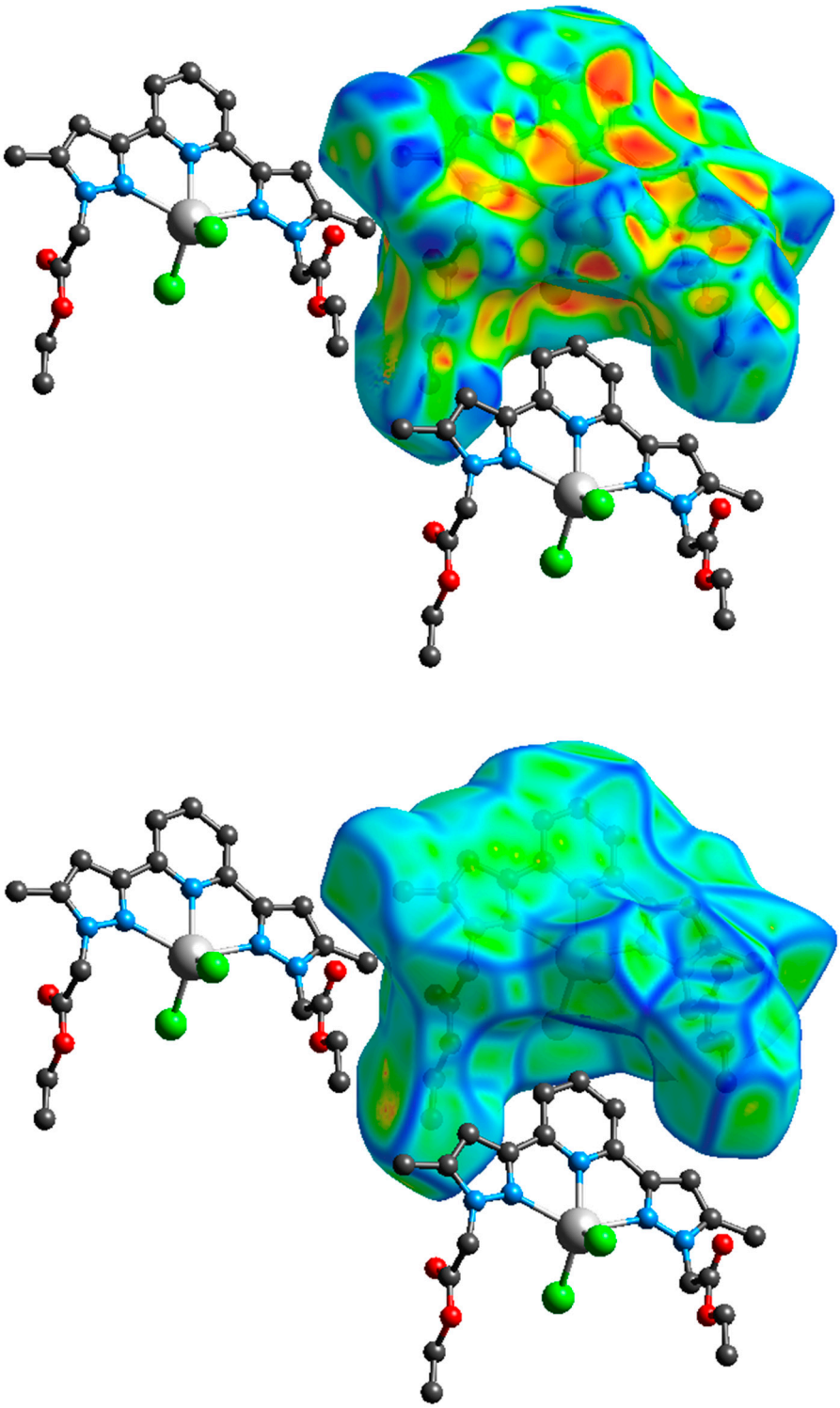

Figure S4: shape index (*top*) and curvedness (*bottom*) of **3.**

8. 2D Fingerprint plots of B, L, 1, 2 and 3

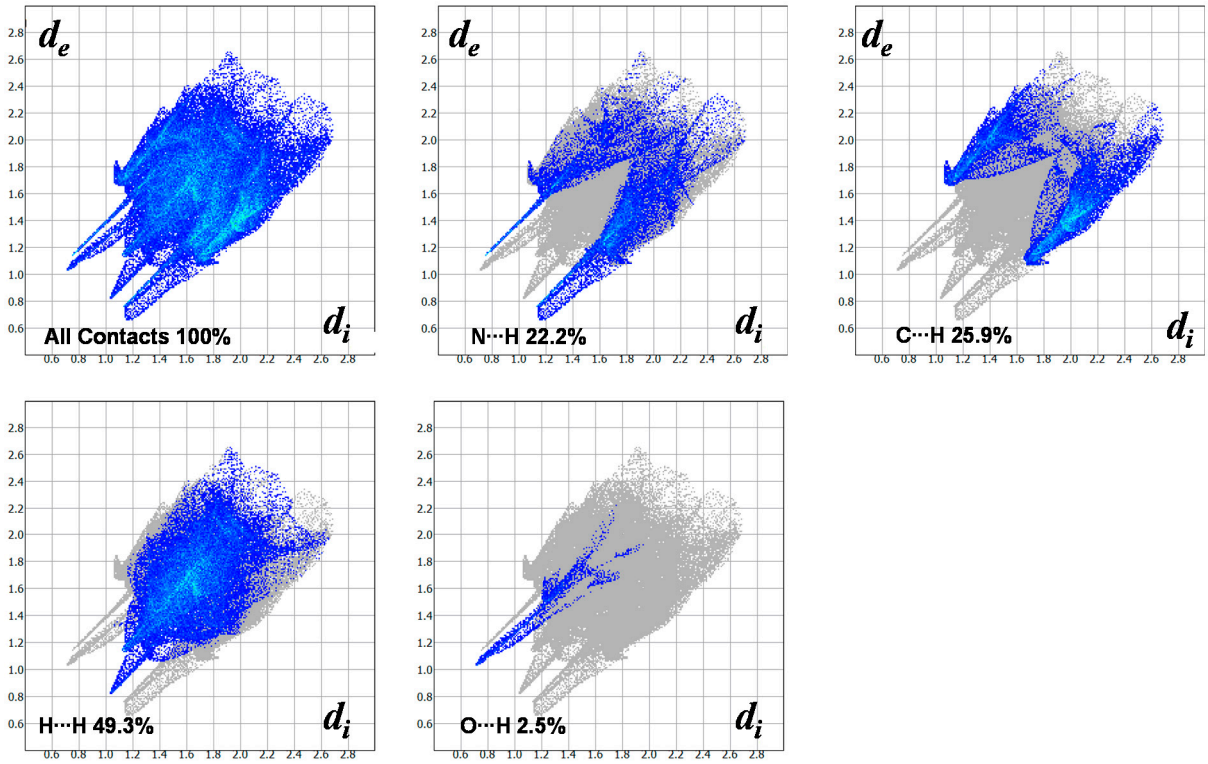

Figure S5: 2D Fingerprint plots derived from Hirshfeld surfaces, displaying various intermolecular interactions for **B**.

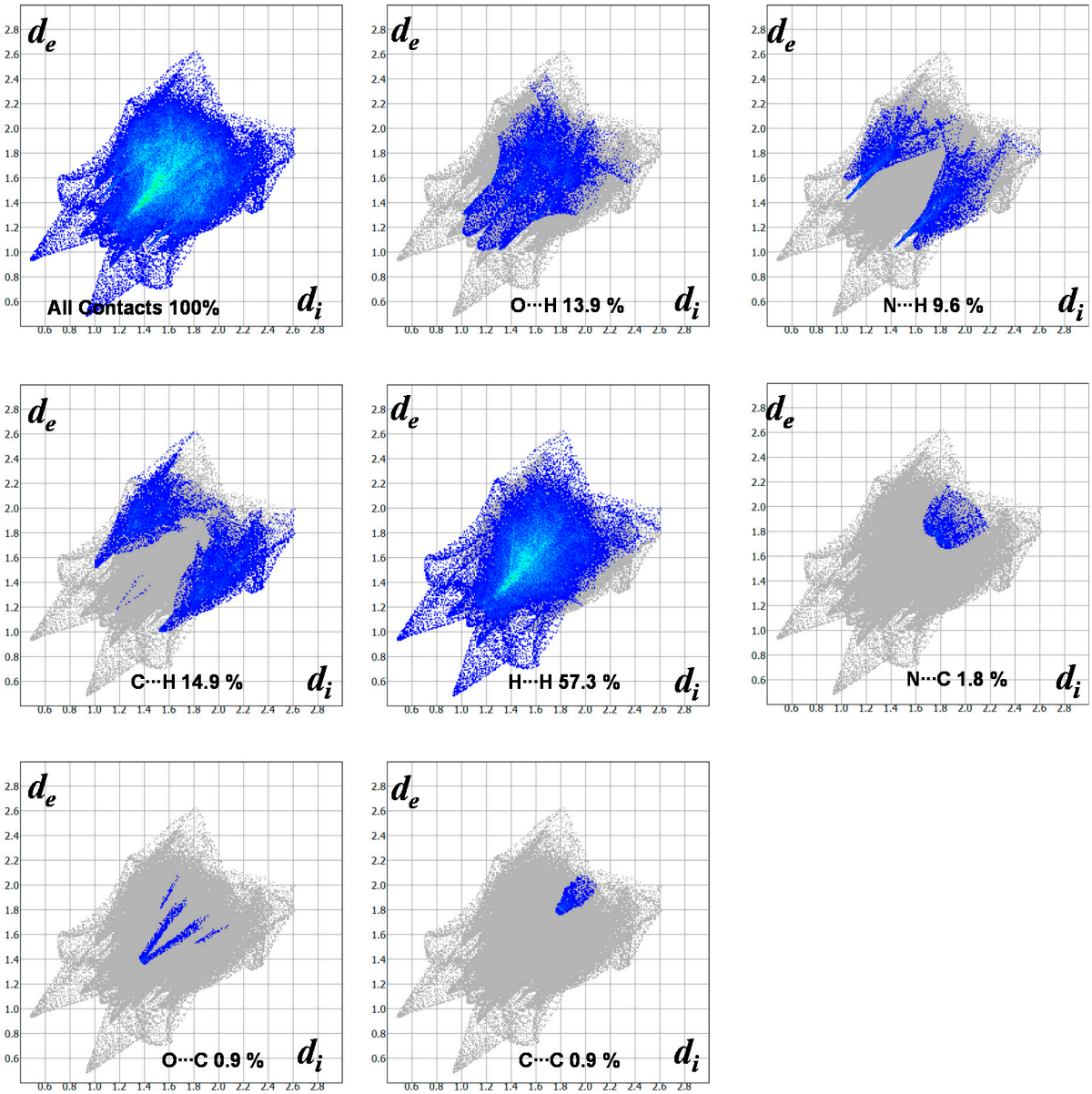

Figure S6: 2D Fingerprint plots derived from Hirshfeld surfaces, displaying various intermolecular interactions for **L**.

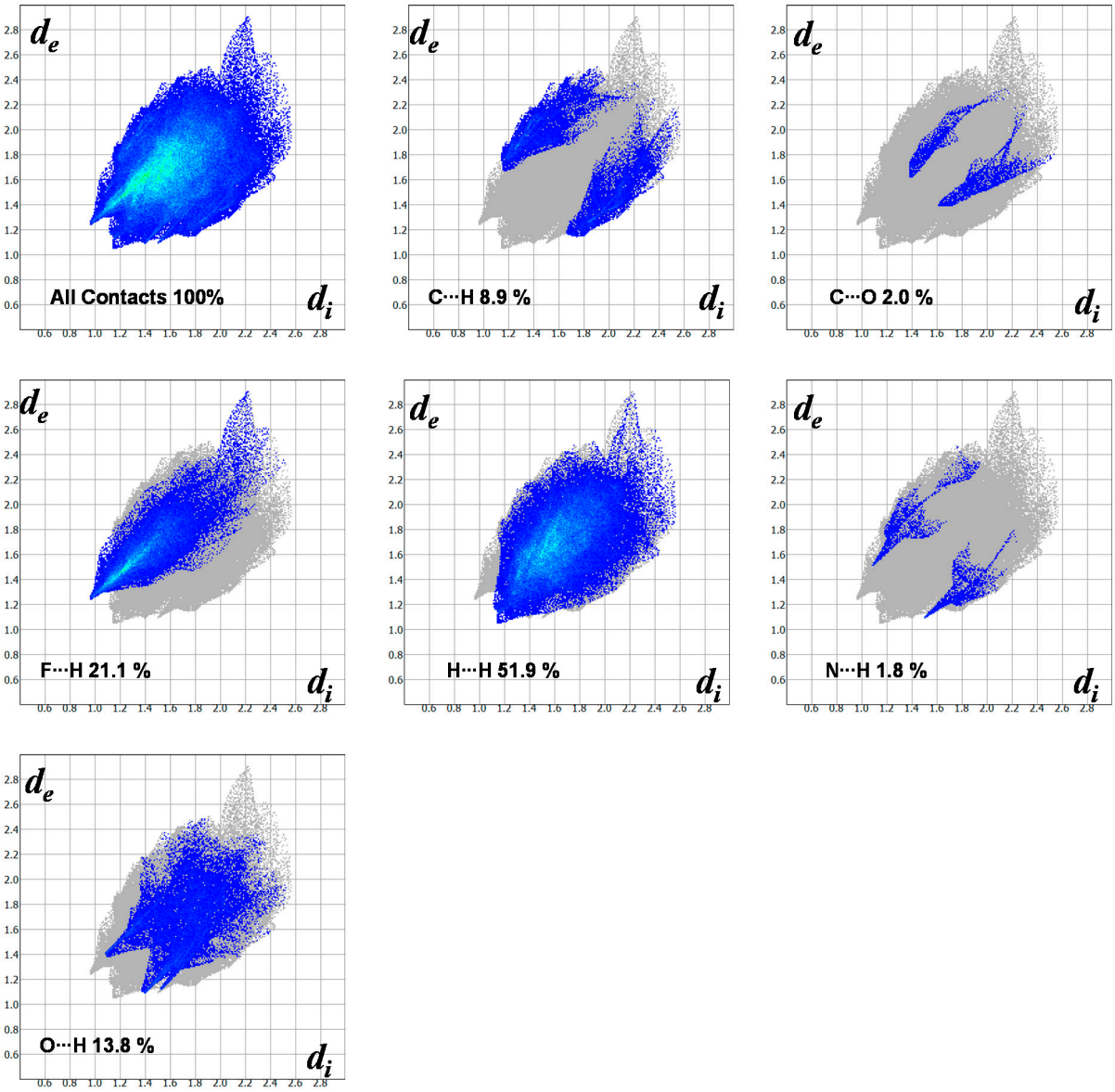

Figure S7: 2D Fingerprint plots derived from Hirshfeld surfaces, displaying various intermolecular interactions for **1**.

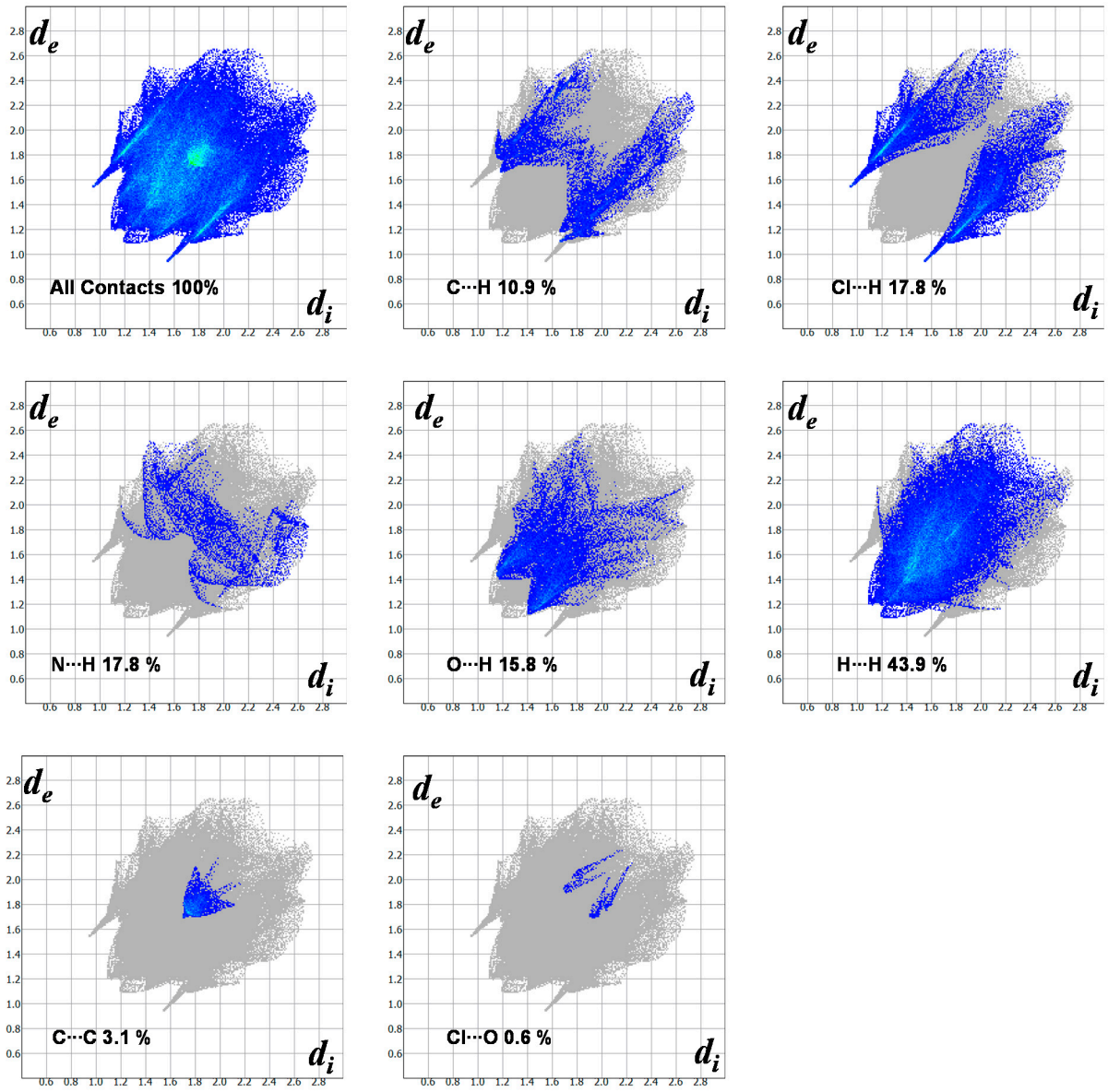

Figure S8: 2D Fingerprint plots derived from Hirshfeld surfaces, displaying various intermolecular interactions for **2**.

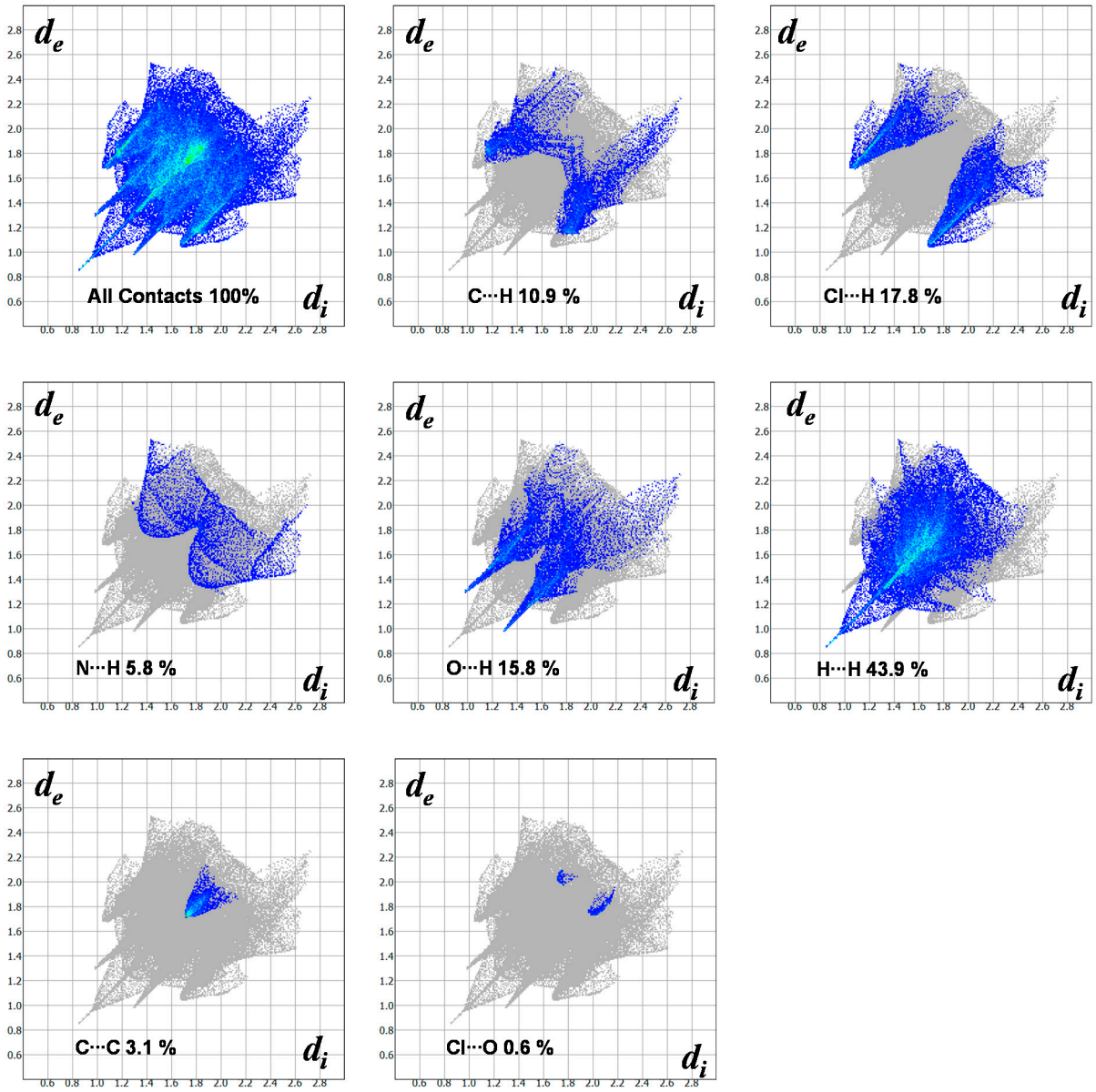

Figure S9: 2D Fingerprint plots derived from Hirshfeld surfaces, displaying various intermolecular interactions for **3**.

9. TGA of L, 1, 2 and 3

The thermogram of **L** revealed its thermal stability until 120°C. Further it undergoes three successive steps of thermal decomposition within temperature ranges of 120–385°C, 385–500°C and 500–800°C (Figure S10). In the first step, the loss of two ethyl acetate molecules (43%), one molecules of each ethane (73%) and methane (4%) from the ligand **L** was observed thus giving a total percentage of 53% fitting very well with the calc. weight loss of 54%. For the second step, a weight loss of ~29% was observed, which could be due to the pyrolysis of **L** into two molecules of propane and water molecules, fitting well with the total percentage of calc. weight loss of 30%. The third step revealed a weight loss of ~40% which could be attributed to the loss of two molecules of pyrazole and one molecule of pyridine fragments of the ligand, which is almost corroborated to the corresponding calc. weight loss of 52%. The coordination compound **1** showed a two-step weight loss: a first one over the range (230-615°C) of ca. 72% which is due to the decomposition of **1** into four ethyl acetate molecules, two ethane molecules, two pyrazole, one pyridine and two trifluoroborane $BF_{3(g)}$ molecules,[37] (total calc. weight loss = 72%). A second step was observed over the range (615-900°C) of 18% which is due to the evolution of two molecules of pyrazole and one molecule of pyridine (total calc. weight loss = 20%) (Figure S11). Coordination compounds **2** and **3** exhibited a different thermogram with a three step weight profile (Figures S12 and S13). In the first step, **2** and **3** showed a weight loss of ~24% (310–380°C) and 23% (270-380°C), respectively, which could be due to the formation of two ethane molecules and one chlorine molecule (total calc. weight loss = 24% and 23% for **2** and **3**, respectively). The second and third steps revealed weight loss of 57% (380-900°C) and 70.6% (380-900°C) for both **2** and **3**. This corresponding weight loss (58.2% in **2** and 72% in **3**) could be due to the loss of ethyl acetate (two molecules each in **2** and **3**), pyrazole (one molecule in **2** and two molecules in **3**), pyridine and water molecules (one molecule each in **3**).

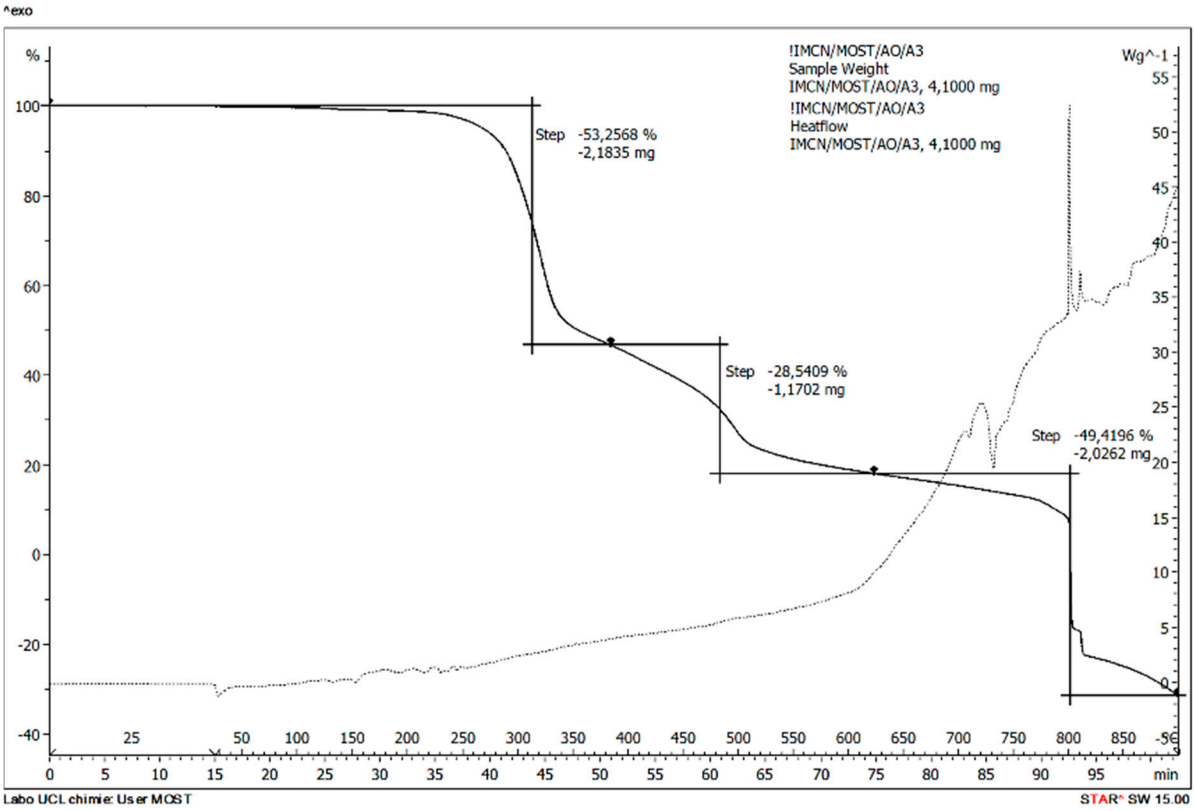

Figure S10: TGA plot of **L**.

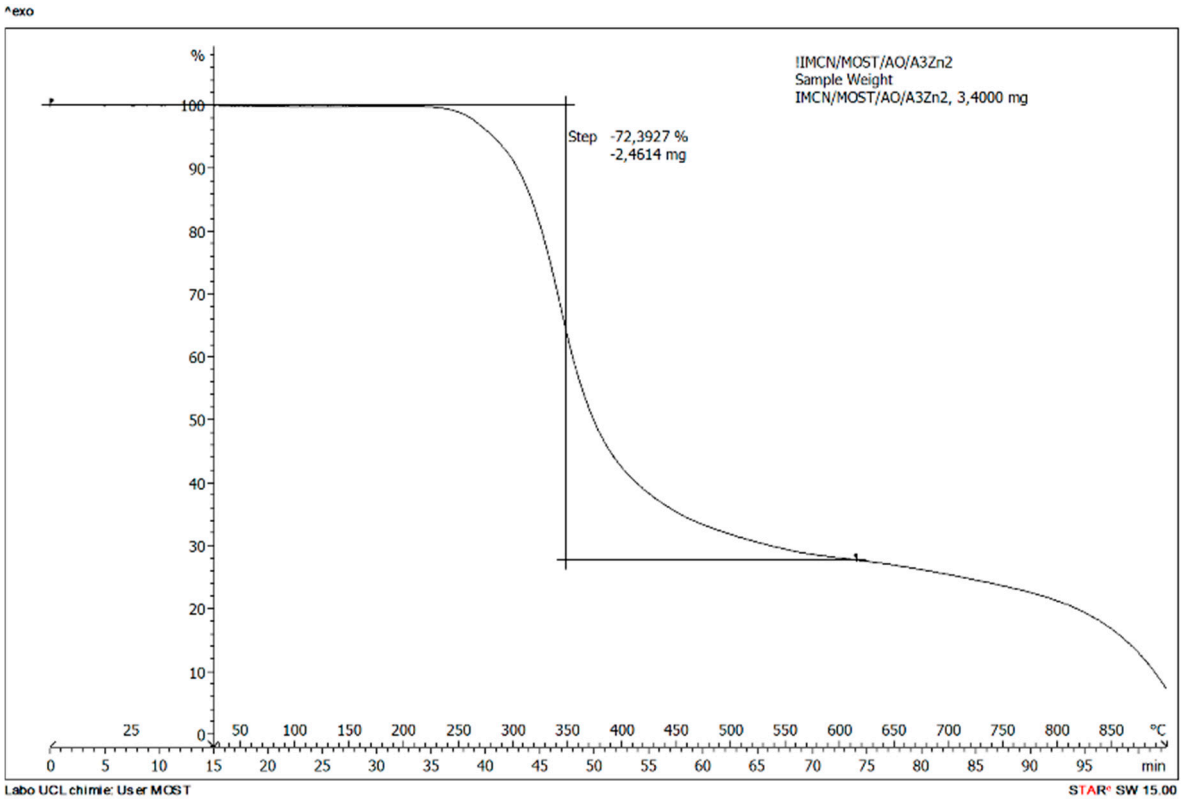

Figure S11: TGA plot of **1**.

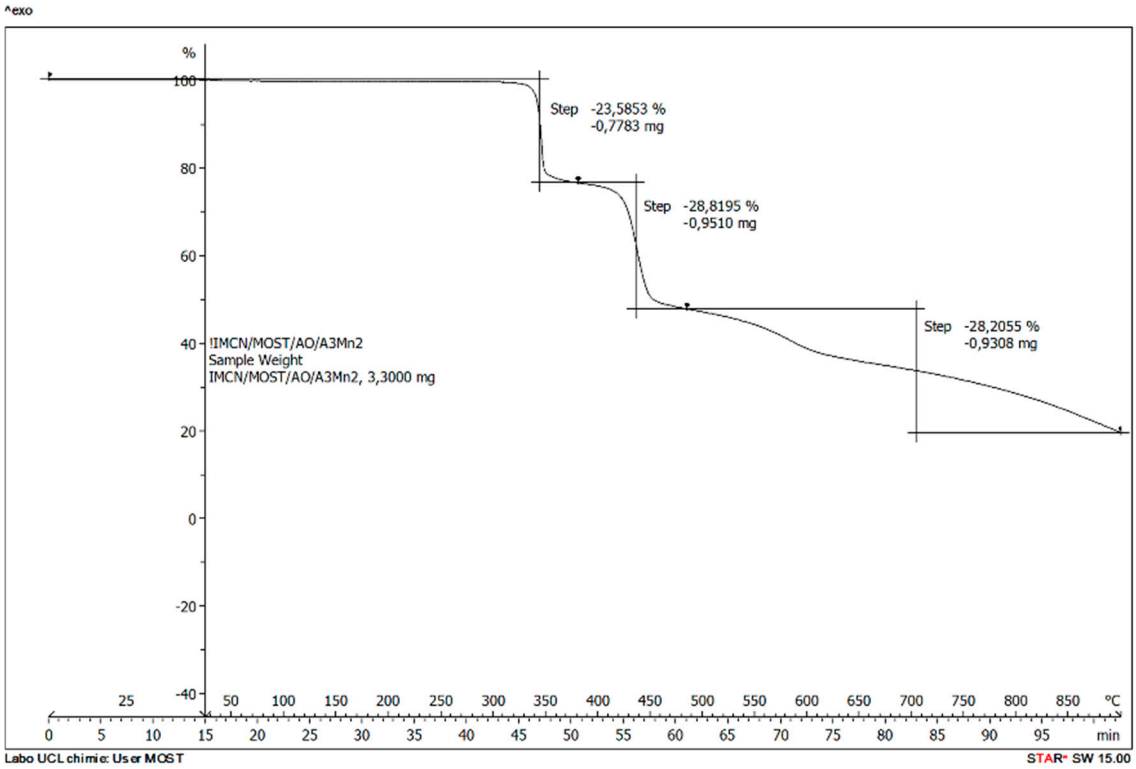

Figure S12: TGA plot of **2**.

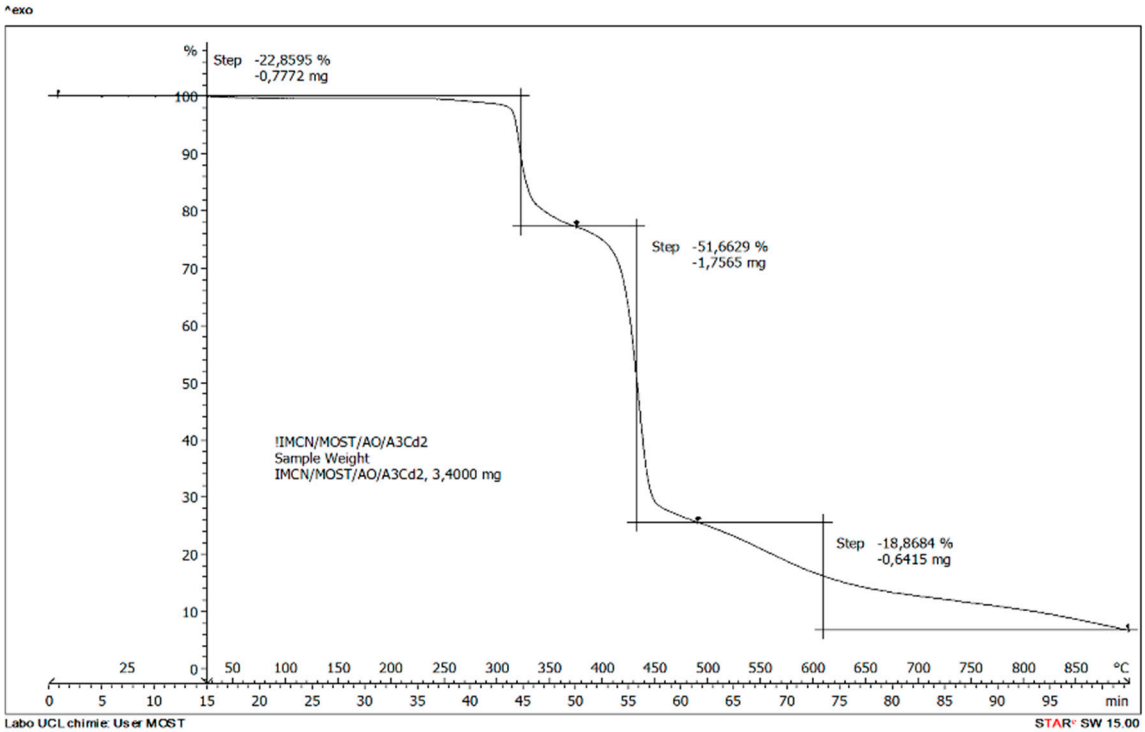

Figure S13: TGA plot of **3**.

10. Ortep plots

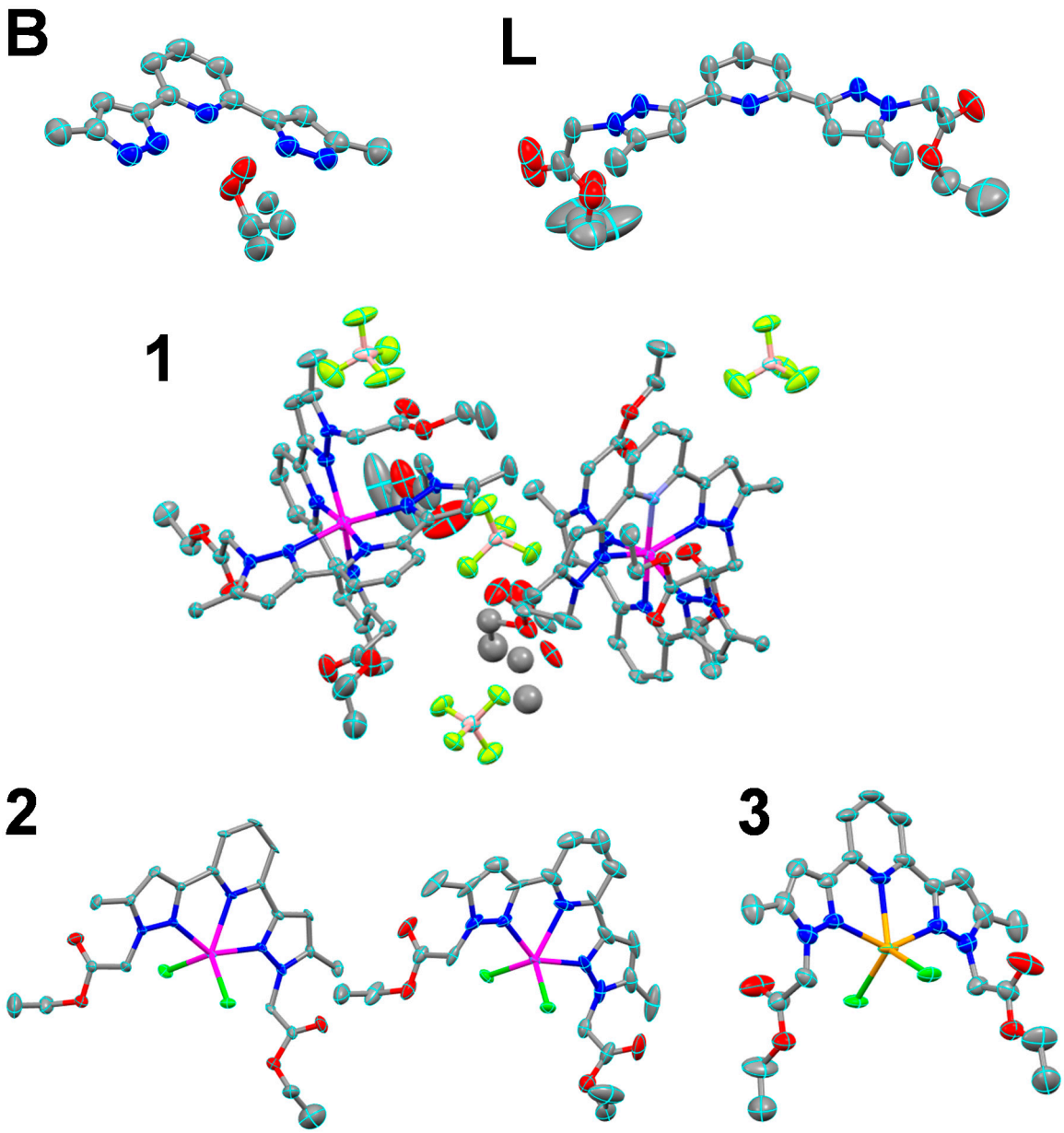

Figure S14: Ortep plots (50% probability level) of all compounds presented in this paper.